

# Mineral reactions in sulphide systems as indicators of evolving fluid geochemistry – a case study from the Apollo mine, Siegerland, FRG

THOMAS WAGNER AND NIGEL J. COOK

Mineralogisches Institut der Universität Würzburg, Am Hubland, D-97074 Würzburg, Germany

## Abstract

The textural and paragenetic relationships of sulphide and sulphosalt minerals within Cu–Pb–Sb–Bi hydrothermal vein mineralization at the Apollo mine, Siegerland, Germany, are interpreted in terms of various reaction sequences. An earlier primary sulphide mineralization hosted within a siderite vein of the Siegerland type, with pyrite, chalcopyrite, sphalerite and galena as main component phases, has been overprinted by Sb-, Bi- and Cu-rich fluids. This superposition resulted in the formation of new quartz–stibnite veins, and various mineral reactions with the primary sulphides including the formation of the sulphosalt minerals semseyite, tetrahedrite, meneghinite, jaskolskiite, boulangerite, bournonite and zinkenite. Based on microprobe analyses of reaction pairs and determination of mineral proportions in some cases, a series of quantitative data for each mineral reaction may be generated. This, in turn, allows for the construction of isocon diagrams permitting the relative mobility and immobility of all chemical elements involved in each reaction to be discussed. Two stages of reactive replacement are identified, characterized by immobile behaviour of S and supply of Sb and Cu during the first stage and relative immobility of S and Sb with no further supply of metals during the second stage. Formation of sulphosalts inside the siderite vein during the first stage is interpreted as a decrease of disequilibrium between hydrothermal fluids and pre-existing vein minerals. Replacement processes of the second stage are interpreted as an equilibration of geochemical contrasts between different points within the siderite vein and also between the siderite and quartz–stibnite vein systems. The geochemical evolution of fluid composition during the entire mineralizing event may therefore be modelled, based on the transfer of chemical components reflected in the succession of mineral reactions. Such an approach has applications to comparable polyphase mineralization sequences, in which an understanding of fluid evolution patterns may greatly assist in the development of genetic models for mineral deposits. Solid-state diffusion and grain-boundary diffusion are considered to be the dominant mechanisms for short-range mass transport, whereas diffusion of ionic and complex species through the fluid is considered to be of major importance in long-range mass transport.

KEYWORDS: sulphide systems, fluid geochemistry, diffusion, Apollo mine, Germany.

## Introduction

HYDROTHERMAL overprinting of a pre-existing sulphide mineralization can often lead to the formation of a new or heavily modified sulphide and sulphosalt assemblage through a series of replacement reactions. This is especially true if the hydrothermal fluid introduced into the system has a chemical character which differs significantly from the earlier mineralization. The sequence of

mineral reactions, therefore, reflects the change in chemical composition of the overprinting fluid. During the replacement process, some chemical elements behave in an immobile fashion while others are extremely mobile (Moëlo *et al.*, 1988; Ni Wen *et al.*, 1991). A quantitative treatment of a series of mineral reactions can thereby help to identify systematic patterns of mobile and immobile behaviour of certain elements within open systems.

*Mineralogical Magazine*, August 1997, Vol. 61, pp. 573–590

© Copyright the Mineralogical Society

At the abandoned Apollo antimony mine, Siegerland, Germany, a primary sulphide mineralization with pyrite, sphalerite, chalcopyrite and galena hosted within a siderite vein of the Siegerland type has been strongly overprinted by Sb-, Bi- and Cu-rich fluids. Reaction resulted in the formation of a complex sulphosalt assemblage in which tetrahedrite, meneghinite, semseyite, jaskolskiite, zinkenite, bournonite and boulangerite are the main components (Wagner and Cook, 1996).

The Apollo mine is located about 25 km NE of Koblenz in the southern part of the Siegerland siderite district, Rhenish Massif (Fig. 1), the deposit being situated at the boundary between Middle Siegenian and Upper Siegenian Devonian sediments (Meyer, 1965; Fenchel *et al.*, 1985). The entire area forms a part of the thrust-fold-belt of the Rhenish Massif, belonging to the externides of the Variscan orogenic belt (Weber and Behr, 1983; Oncken, 1984; Franke and Oncken, 1990). The major tectonic elements show a general SW–NE strike with the main fold axes dipping about 10–15° towards the NE. The tectonic position of the vein mineralization itself is on the southeastern flank of a minor anticline forming a part of the Siegen main anticline, a major antichinal zone. Most of the folded rocks are displaced by intense thrusting with a few major

thrust zones and many minor thrusts (Oncken, 1984). The Siegen Main Thrust, one of the most important thrust zones of the Rhenish Massif, occurs about 5 km NW of the Apollo mine.

Two spatially related parageneses occur as individual vein systems. These are (I) siderite veining of the Siegerland type; a single massive vein of about 0.7 to 1.1 m in thickness striking N–S and dipping very steeply towards the W, and (II) younger quartz–stibnite vein mineralization, represented by a network of many small veins and veinlets of 1 to 30 cm in thickness. Veining of the siderite mineralization is related to the principal deformation event of the Variscan orogeny (Walther, 1982; Fenchel *et al.*, 1985; Hein, 1993). The vein system of the quartz–stibnite mineralization is younger than the siderite vein. Both textural relationships and fluid inclusion data indicate a late-Variscan age which can be related to the extensional collapse of the Variscan orogenic belt (Perichaud, 1980; Behr *et al.*, 1987; Boiron *et al.*, 1990; Couto *et al.*, 1990; Munoz *et al.*, 1992; Ortega and Vindel, 1995). This younger, presumably lower Permian, mineralizing event led to the contemporaneous formation of the new quartz–stibnite vein system and the hydrothermal overprinting of the pre-existing sulphides of the siderite vein.

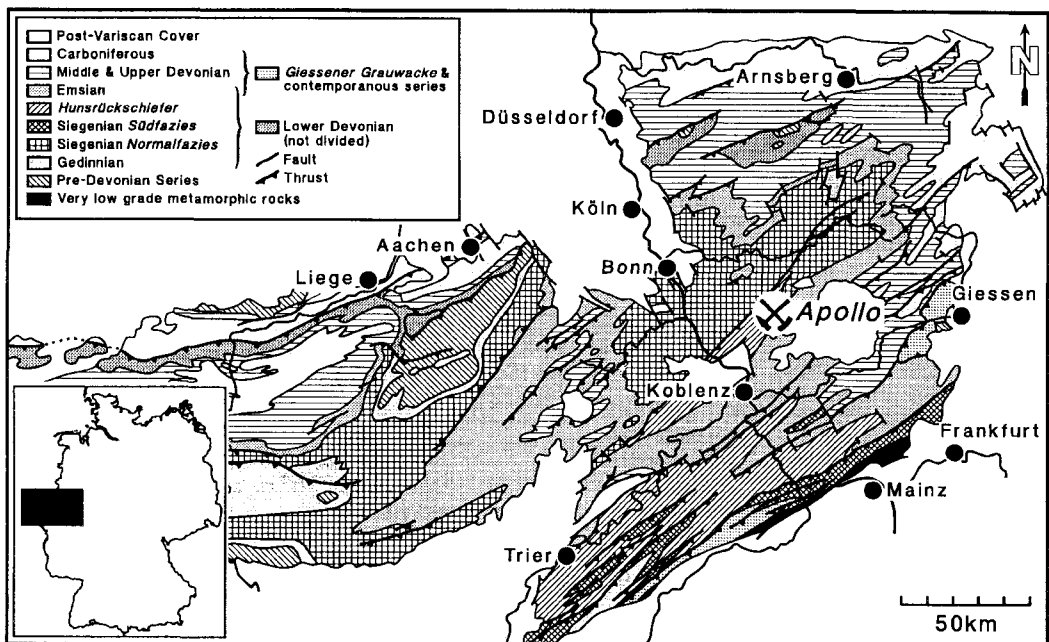


FIG. 1. Geological sketch map of the Rhenish Massif showing the location of the Apollo deposit. Redrawn and slightly modified after von Koenigswald and Meyer (1994).

### Mineralogy and textures

Comparison of structural and textural relationships of the quartz-stibnite assemblage and the assemblage of the siderite vein indicates distinct development stages. Mineralization of the quartz-stibnite vein is related to the late-Variscan event (stibnite stage) only. In contrast, mineralization of the siderite vein contains readily recognizable assemblages of the Variscan siderite stage (pyrite, siderite, quartz), the Variscan sulphide stage (pyrite, sphalerite, chalcopyrite, galena) as well as of the overprinting late-Variscan stibnite stage (tetrahedrite, semseyite, meneghinite, jaskolskiite, bournonite, boulangerite). Textures of assemblages of the siderite stage and the sulphide stage are in complete agreement with published relationships from other siderite veins of the Siegerland (Fenchel *et al.*, 1985; Hein, 1993) and are, therefore, not explained in detail in the following description.

The quartz-stibnite assemblage is characterized by a sequential precipitation of minerals at the beginning, and an intensive replacement during the formation of various Sb-sulphosalts in the later stage. An intensive pyritization and a coarsening of quartz grains in the immediate wallrock is associated with the mineralizing event of the stibnite-stage mineralization. Chlorite is the first mineral to form inside the vein system and coats the walls of the individual veins. Chlorite is followed by quartz which is the main constituent of the veins. Quartz has grown from the walls of the veins towards the centre with the crystallographic *c*-axes perpendicular to the walls. It has, however, not completely filled the veins and most quartz crystals show idiomorphic terminations. The resulting open space in the central part of each vein is filled by stibnite and later sulphosalts. Zinkenite is somewhat younger than stibnite and forms reaction rims around that mineral (Fig. 2a) and replacement zones within the stibnite; the replace-

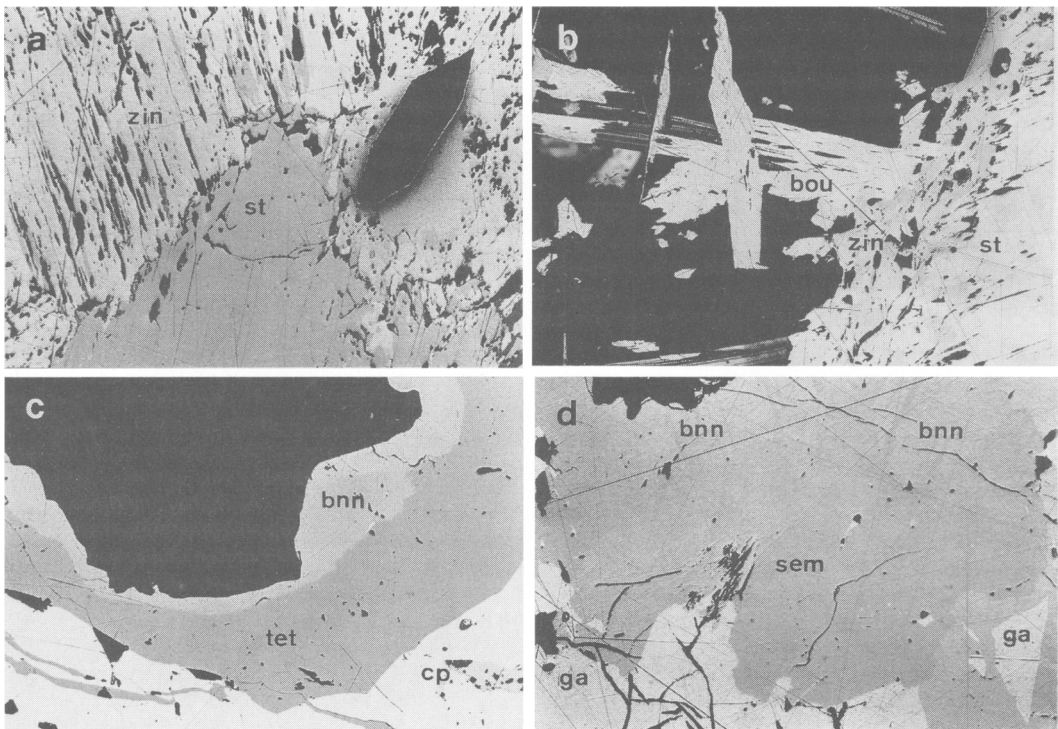


FIG. 2. Photomicrographs in reflected light showing replacement textures of sulphides and sulphosalts from the Apollo mine. (a) Simple reaction rim of zinkenite (zin) around stibnite (st); reaction (1); quartz-stibnite vein. Width of field, 690  $\mu\text{m}$ . (b) Acicular crystals of boulangerite (bou) have replaced zinkenite (zin); reaction (2); quartz-stibnite vein. Width of field, 540  $\mu\text{m}$ . (c) Complex reaction rim of tetrahedrite (tet) and bournonite (bnn) around chalcopyrite (cp). Tetrahedrite has replaced chalcopyrite and is in turn replaced by bournonite; reactions (3) and (4); siderite vein. Width of field, 620  $\mu\text{m}$ . (d) Reaction rim of semseyite (sem) around galena (ga) with a portion of semseyite already replaced by bournonite (bnn); reaction (5) and (6); siderite vein. Width of field, 530  $\mu\text{m}$ .

ment starting from minor cracks and grain boundaries. Boulangerite is the youngest mineral of the assemblage and forms small reaction rims around zinkenite (Fig. 2*b*) and individual aggregates which indicate almost complete replacement of zinkenite.

Textural relationships of the stibnite-stage mineralization superimposed on the siderite vein are appreciably more complicated. The formation of reaction products due to hydrothermal overprinting depends not only on the bulk composition of the mineralizing fluid but also on the compositions of the pre-existing sulphides. Formation of tetrahedrite is thus restricted to chalcopyrite-rich parts of the vein whereas formation of a range of Pb-Sb-sulphosalts without Cu, such as semseyite or boulangerite, is restricted to galena-rich parts. A comprehensive account of mineral chemistry, including unusual Bi-rich varieties of various sulphosalt minerals, has been given by Wagner and Cook (1996).

*Tetrahedrite* is the oldest mineral within the sulphosalt assemblage of the siderite vein and is closely associated with bournonite and sphalerite. It forms the inner part of zoned reaction rims around chalcopyrite veinlets. Reactive replacement commenced either from grain boundaries between chalcopyrite and the host siderite or from minor extensional cracks within chalcopyrite. In most cases, the replacement of chalcopyrite is incomplete with the formation of only a narrow reaction rim about 10–20  $\mu\text{m}$  in size. In some cases, however, the replacement is pervasive, leading to the formation of a breccia-like texture with isolated relicts of chalcopyrite enclosed within tetrahedrite. Corroded grain contours of these chalcopyrite relicts indicate the formation by a replacement process and not by a process of mechanical brecciation. Initial replacement of chalcopyrite by tetrahedrite is followed by a second replacement process with the formation of reaction rims of bournonite enclosing the tetrahedrite rims (Fig. 2*c*). Iron-rich primary sphalerite of the sulphide stage has been mobilized during replacement. This has partially recrystallized as Fe-poor second generation sphalerite as fillings of extensional cracks mainly in chalcopyrite. A minor amount of the zinc of this mobilized sphalerite is first incorporated in tetrahedrite and then reprecipitated during subsequent decomposition of tetrahedrite.

*Semseyite* forms reaction rims around primary galena, especially along the grain boundaries between coarse galena and coarse pyrite. Additionally, some minor veinlets of galena are almost completely replaced by semseyite with only isolated relict grains of galena preserved within the massive semseyite aggregates. Most semseyite shows a caries texture against galena whereas pyrite grains in contact with semseyite, which are not affected by the replacement process, show well-preserved

idiomorphic crystal morphologies. The initial replacement reaction resulting in the formation of semseyite is followed by the formation of either bournonite or boulangerite in a second reaction, leading to complex zoned reaction rims similar to textural relationships in chalcopyrite-rich areas of the vein. Boulangerite forms sprays and clusters of acicular crystals, 50–250  $\mu\text{m}$  in size, which occur as minor reaction rims around semseyite (Fig. 3*a*). Boulangerite formation is most intensive along the grain boundaries between coarse galena and coarse pyrite, but some smaller aggregates of boulangerite also occur as rims surrounding massive semseyite veinlets. Bournonite preferentially replaces the massive semseyite veinlets and shows a well-developed caries texture against semseyite (Fig. 2*d*). Bournonite is often associated with second generation pyrite, which occurs as groups or aggregations of crystals and grains, typified by rounded grain contours.

*Meneghinite* occurs as reaction rims around primary galena, with the reactive replacement starting from the grain boundaries between galena and siderite (Fig. 3*b*). The grain contacts between meneghinite and galena show a well-developed caries texture. However, these are only sparsely preserved because most meneghinite has decomposed to a myrmekitic intergrowth assemblage of bournonite and galena in the second stage of the replacement reaction sequence (Fig. 3*c*). The resulting textures show groups of subparallel-oriented crystals of meneghinite, or isolated relict meneghinite grains with xenomorphic grain shapes, in a myrmekitic assemblage of bournonite and galena (Fig. 3*d*). Several stages of this decomposition reaction are well documented in the textures of the siderite vein. A directly comparable decomposition reaction has been previously described by Ni Wen *et al.* (1991) but no indication for the formation of meneghinite from primary galena has been mentioned by these authors. Portions of uncorroded meneghinite in contact with portions which are almost completely decomposed to the myrmekitic assemblage, indicate that the replacement was restricted to certain areas of the vein. In some cases, the former grain boundaries between galena and meneghinite have acted as a fluid channel, leading to an almost complete decomposition of meneghinite in these areas. Some groups of meneghinite crystals, which are well preserved along cleavage planes in siderite, show an intergrowth with the rare Cu-Pb-Sb-Bi sulphosalt jaskolskiite.

### Mineral reactions

*Principles.* Hydrothermal overprinting of the pre-existing sulphide assemblages is characterized by

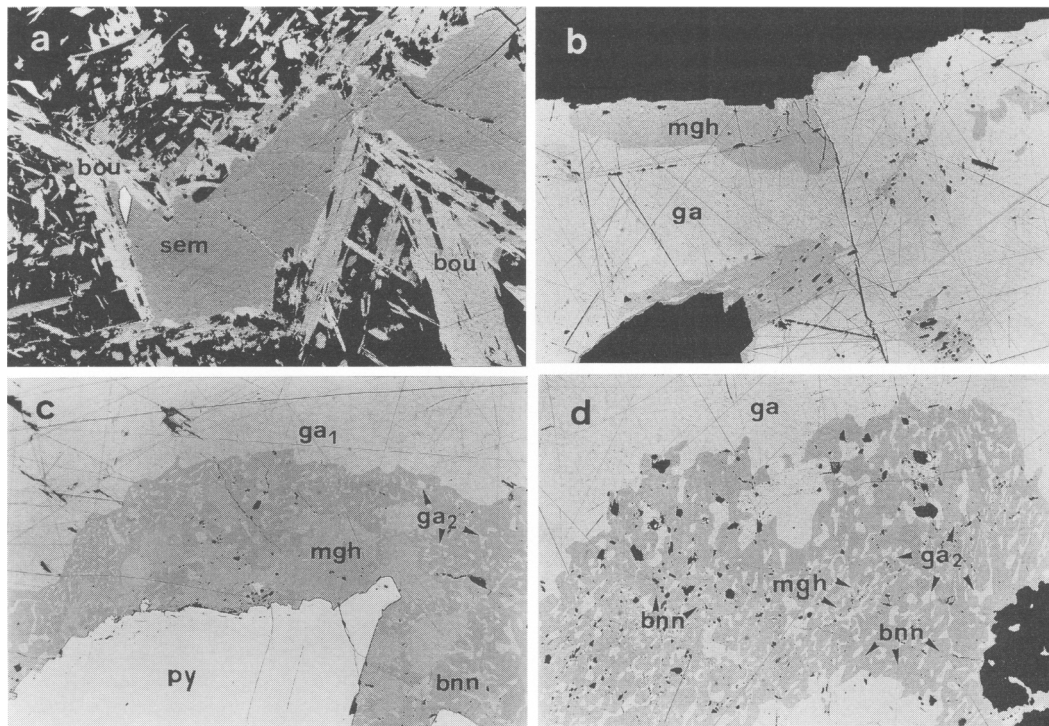


FIG. 3. Photomicrographs in reflected light showing replacement textures of sulphides and sulphosalts from the Apollo mine. (a) Semseyite (sem) has decomposed to clusters of acicular boulangerite (bou); reaction (7); siderite vein. Width of field, 610  $\mu\text{m}$ . (b) simple reaction rim of meneghinite (mgh) around and locally within galena (ga); reaction (8); siderite vein. Width of field, 950  $\mu\text{m}$ . (c) Well-developed caries texture between primary galena ( $ga_1$ ) and meneghinite (mgh). Most of the latter has decomposed to a myrmekitic assemblage of bournonite (bnn) and secondary galena ( $ga_2$ ); reaction (9); siderite vein. py: pyrite. Width of field, 1.27 mm. (d) Final stage of the replacement process, in which only fine-grained relicts of meneghinite remain within the assemblage of intergrown bournonite (bnn) and secondary galena ( $ga_2$ ); reaction (9); siderite vein. Width of field, 1.36 mm.

reactions of solid phases with the evolving mineralizing fluid phase. Therefore, an open-system behaviour can generally be assumed for certain elements in the replacement processes. Textural relationships, especially zoned reaction rims, indicate incomplete reactions and disequilibrium conditions during all stages of the replacement processes preserved in samples from the Apollo mine. A quantitative treatment of the mineral reactions can therefore only be performed by a method based on the calculations derived by Gresens (1967) for metasomatic alteration. The isocon-method developed by Grant (1986) is particularly well suited for application in the present case, because the methodology is relatively simple and the main disadvantage of the method, the difficulty to apply to alteration profiles or alteration gradients, does not matter here. The applicability of the isocon-method

to opaque-mineral reactions has been previously demonstrated by Ni Wen *et al.* (1991).

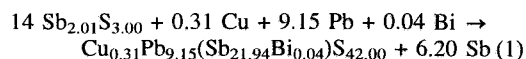
**Methodology.** Compositions of the mineral reaction pairs were analyzed by wavelength-dispersive electron microprobe; the analyses were carried out on the CAMECA SX-50 instrument in Würzburg. Operating conditions were 15 kV at a beam current of 15 nA and a beam size of 1–2  $\mu\text{m}$ . Standards and radiations used were as follows: pure Cu ( $K\alpha$ ), pure Bi ( $M\alpha$ ), pure Ag ( $L\alpha$ ), pure Te ( $L\alpha$ ), pure  $\text{FeS}_2$  (Fe- $K\alpha$ , S- $K\alpha$ ), pure ZnS ( $K\alpha$ ), pure  $\text{Sb}_2\text{S}_3$  ( $L\alpha$ ) and pure PbS ( $M\alpha$ ).

Calculation procedures for the quantitative treatment of the mineral reactions were carried out in the following manner. Mean compositional values from the microprobe analyses of reaction pairs were recalculated to a common S-basis for both initial and final (product) material. In the following

discussion of mineral reactions, relevant microprobe data for each reaction and other quantitative data are given in Tables 1a to 9a and 1b to 9b, 9c respectively. Atomic concentrations of initial and final compositions were plotted on an isocon diagram (Grant, 1986). Isocons were chosen as a graphical best-fit in cases with two or more chemical elements defining an isocon. In cases in which no two-element isocon was detectable, S was chosen to be the immobile element with respect to the classical diffusion-model for sulphides (Birchenall, 1974) as a first approximation. The slope of the isocon was corrected by the quotient of the total number of atoms per formula unit in the initial and final compositions to give the stoichiometric factor for each reaction. In cases with more than a single reaction product, the decomposition reaction of meneghinite to the myrmekitic assemblage bournonite-galena in particular, the volume percentages of bournonite and galena in the myrmekite were determined by a VIDS V image analysing system. The volume percentages were corrected with the volumes per 24 S-atoms (given in Å<sup>3</sup>) to give percentages on 24-S basis (Ni Wen *et al.*, 1991).

*Application.* The reaction sequence *stibnite* → *zinkenite* → *boulangerite* is the only replacement process identified from preserved textures within the quartz-stibnite vein system. Reaction rims of zinkenite around stibnite are quite common in the

assemblage and have formed by the reaction *stibnite* + *fluid* → *zinkenite* + *fluid*. Initial and final compositions (Table 1a) were recalculated on a common 42-S basis (Table 1b). The isocon diagram (Fig. 4a) shows no evidence of a two-element-isocon, so S is therefore treated as the single relatively immobile element. A strong supply of Pb and removal of Sb during the reaction process can be assumed. Cu and Bi are not present in significant amounts in either the initial or final (product) phase, but have been plotted on the isocon diagram for comparison with the other reactions. The overall reaction can be summarized as:



The replacement reaction *zinkenite* + *fluid* → *boulangerite* + *fluid* is only sparsely documented in preserved textures and is exposed as minor reaction rims of boulangerite around stibnite. Initial and final compositions (Table 2a) were recalculated to a common 462-S basis (Table 2b). The resulting isocon diagram (Fig. 4b) for the reaction gives no indication of a two-element isocon and, therefore, S is again chosen as the relatively immobile element. If this assumption is valid, a supply of Pb and a loss of Sb can be deduced, which is in agreement with the reaction (1) above. The resulting reaction can be written as:

TABLE 1a. Average electron-microprobe analyses for the reaction pair stibnite, zinkenite

	Stibnite (wt.%), n = 10	Zinkenite (wt.%), n = 10	Stibnite (atom %)	Zinkenite (atom %)
Cu	0.08	0.33	0.09	0.42
Pb	0	31.49	0	12.46
Sb	70.82	44.35	40.09	29.88
Bi	0.09	0.15	0.03	0.05
S	27.80	22.36	59.78	57.19
Total	98.79	98.68	99.99	100.00

TABLE 1b. Quantitative data for the reaction stibnite + fluid → zinkenite + fluid

Element	Stibnite	Factor	Initial	Zinkenite	Factor	Final	Difference
Cu	0	14.00	0	0.31	1.00	0.31	0.31
Pb	0		0	9.15		9.15	9.15
Sb	2.01		28.14	21.94		21.94	-6.20
Bi	0		0	0.04		0.04	0.04
S	3.00		42.00	42.00		42.00	0

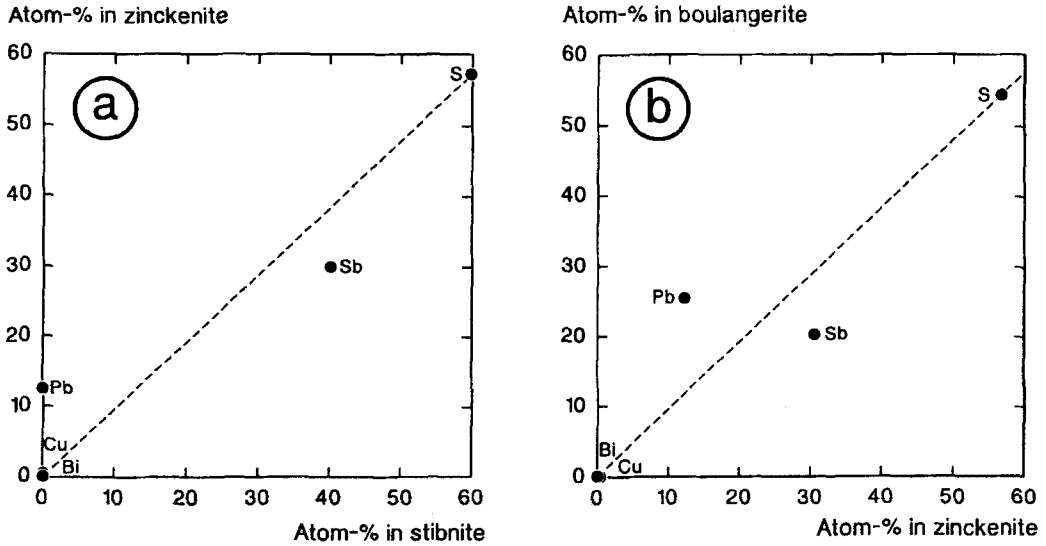
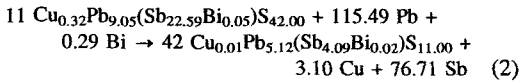


FIG. 4. Series of isocon diagrams for zoned reaction rims around stibnite. (a) Formation of zinckenite; reaction (1). (b) Subsequent formation of boulangerite from zinckenite; reaction (2).



Zoned reaction rims around chalcopyrite have formed by the reaction sequence *chalcopyrite* → *tetrahedrite* → *bourmonite*. The first replacement

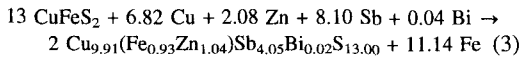
TABLE 2a. Average electron-microprobe analyses for the reaction pair zinckenite, boulangerite

	Zinckenite (wt. %), n = 10	Boulangerite (wt. %), n = 6	Zinckenite (atom %)	Boulangerite (atom %)
Cu	0.33	0.04	0.43	0.06
Pb	30.81	54.71	12.23	25.30
Sb	45.17	25.67	30.52	20.20
Bi	0.18	0.23	0.07	0.11
S	22.12	18.18	56.75	54.33
Total	98.61	98.83	100.00	100.00

TABLE 2b. Quantitative data for the reaction zinckenite + fluid → boulangerite + fluid

Element	Zinckenite	Factor	Initial	Boulangerite	Factor	Final	Difference
Cu	0.32	11.00	3.52	0.01	42.00	0.42	-3.10
Pb	9.05		99.55	5.12		215.04	115.49
Sb	22.59		248.49	4.09		171.78	-76.71
Bi	0.05		0.55	0.02		0.84	0.29
S	42.00		462.00	11.00		462.00	0

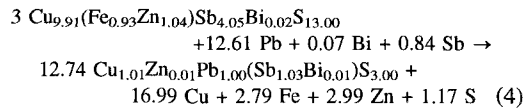
reaction *chalcopyrite + fluid* → *tetrahedrite + fluid* is preserved in the inner parts of these rims. Both the initial and final compositions were recalculated to a common 26-S basis (Table 3a,b). The isocon diagram (Fig. 5b) constructed for the tetrahedrite-forming reaction, shows no two-element isocon, so that if S is treated as the only relatively immobile element, an influx of Cu, Zn and Sb can be assumed. The overall reaction can be written as:



Supply of Zn to the local system is supported by the breakdown and the mobilization of primary Fe-rich sphalerite, whereas Cu and Sb must have been present in the mineralizing fluids at significant concentrations. Fe has been removed from the chalcopyrite aggregates to form later generation pyrite.

The second replacement process, involving formation of bournonite by the reaction *tetrahedrite + fluid* → *bournonite + fluid*, displays a rather different characteristic, with a two-element isocon of Sb and S (Fig. 5b). Therefore, Sb and S can be treated as relatively immobile, whereas Fe, Zn and Cu were removed from, and Pb added to the local system. The removal of Zn has led to the formation of Fe-poor

second generation sphalerite which has approximately the same age as bournonite in the paragenetic sequence (Wagner and Cook, 1996). The analyses were recalculated to a common 39-S basis for both bournonite and tetrahedrite (Table 4a,b). The overall reaction can be written as:



Zoned reaction rims around, and replacement zones in, galena show two distinct reaction sequences; A) *galena* → *semseyite* → *bournonite*, and B) *galena* → *semseyite* → *boulangerite*. The reaction *galena + fluid* → *semseyite + fluid* is preserved very frequently in the vein textures. The corresponding isocon diagram (Fig. 6a) indicates relative immobility of S and Bi, a strong supply of Sb and a loss of Pb during the reaction. Analyses of the initial and final (product) compositions (Table 5a) were recalculated to 21 S atoms (Table 5b). The resulting reaction can be written as:

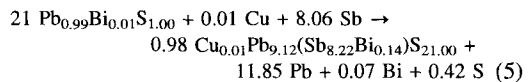


TABLE 3a. Average electron-microprobe analyses for the reaction pair chalcopyrite, tetrahedrite

	Chalcopyrite (wt. %), n = 4	Tetrahedrite (wt. %), n = 4	Chalcopyrite (atom %)	Tetrahedrite (atom %)
Cu	34.23	37.33	25.04	34.24
Fe	29.89	3.08	24.89	3.21
Zn	0.03	4.04	0.02	3.59
Sb	0.02	29.21	0	13.98
Bi	0.09	0.21	0.02	0.05
S	34.48	24.71	50.01	44.91
Total	98.74	98.58	99.98	99.98

TABLE 3b. Quantitative data for the reaction chalcopyrite + fluid → tetrahedrite + fluid

Element	Chalcopyrite	Factor	Initial	Tetrahedrite	Factor	Final	Difference
Cu	1.00	13.00	13.00	9.91	2.00	19.82	6.82
Fe	1.00		13.00	0.93		1.86	-11.14
Zn	0		0	1.04		2.08	2.08
Sb	0		0	4.05		8.10	8.10
Bi	0		0	0.02		0.04	0.04
S	2.00		26.00	13.00		26.00	0

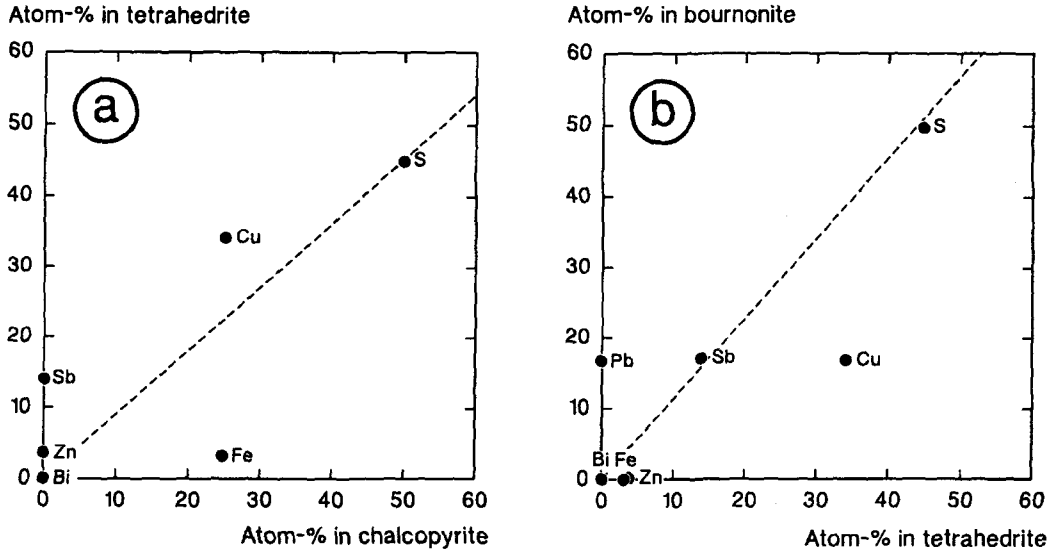


FIG. 5. Series of isocon diagrams for zoned reaction rims around chalcopyrite. (a) Formation of tetrahedrite; reaction (3). (b) Subsequent formation of bournonite from tetrahedrite; reaction (4).

TABLE 4a. Average electron-microprobe analyses for the reaction pair tetrahedrite, bournonite

	Tetrahedrite (wt. %), n = 4	Bournonite (wt. %), n = 4	Tetrahedrite (atom %)	Bournonite (atom %)
Cu	37.33	12.84	34.24	16.66
Fe	3.08	0.01	3.21	0.01
Zn	4.04	0.07	3.61	0.09
Pb	0	41.71	0	16.59
Sb	29.21	25.08	13.98	16.97
Bi	0.21	0.23	0.06	0.09
S	24.71	19.29	44.92	49.59
Total	98.58	99.23	100.02	100.00

TABLE 4b. Quantitative data for the reaction tetrahedrite + fluid  $\rightarrow$  bournonite + fluid

Element	Tetrahedrite	Factor	Initial	Bournonite	Factor	Final	Difference
Cu	9.91	3.00	29.73	1.01	12.61	12.74	-16.99
Fe	0.93		2.79	0		0	-2.79
Zn	1.04		3.12	0.01		0.13	-2.99
Pb	0		0	1.00		12.61	12.61
Sb	4.05		12.15	1.03		12.99	0.84
Bi	0.02		0.06	0.01		0.13	0.07
S	13.00		39.00	3.00		37.83	-1.17

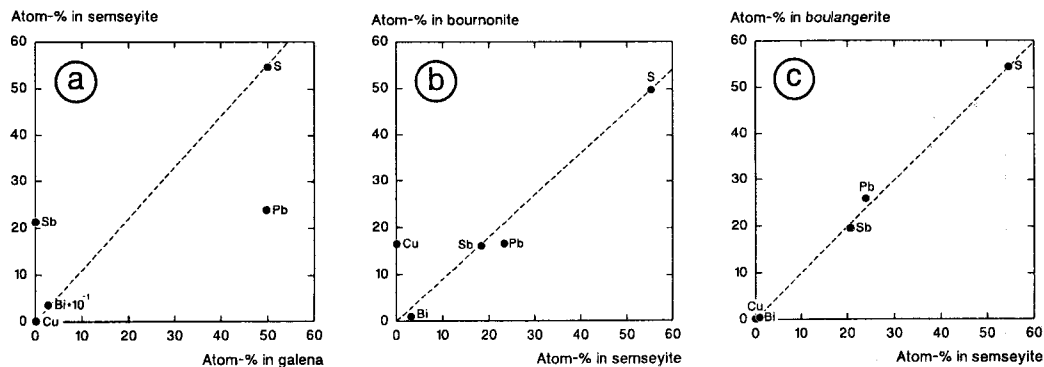
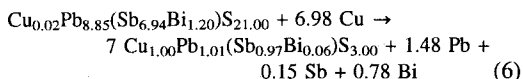


FIG. 6. Series of isocron diagrams for zoned reaction rims around galena. (a) Formation of semseyite; reaction (5). (b) Subsequent formation of bournonite from semseyite; reaction (6). (c) Later formation of boulangerite instead of bournonite; reaction (7).

Pertinent data (Tables 6a,b) and the isocron diagram (Fig. 6b) for the reaction *semseyite* + *fluid* → *bournonite* + *fluid* suggests the relative immobility of both Sb and S, which is in coincident with the behaviour of these elements during the reaction tetrahedrite → bournonite. A significant influx of Cu and removal of Bi and Pb is inferred, so that both Cu and Pb display inverse behaviour in comparison with the tetrahedrite-bournonite reaction. The overall reaction can be written as:



The replacement reaction *semseyite* + *fluid* → *boulangerite* + *fluid* is restricted to galena-rich and chalcopyrite-poor portions of the siderite vein. The relatively immobile behaviour of Sb and Bi can be deduced from the isocron diagram constructed for the reaction (Fig. 6c), thus being in agreement with the

TABLE 5a. Average electron-microprobe analyses for the reaction pair galena, semseyite

	Galena (wt. %), n = 6	Semseyite (wt. %), n = 9	Galena (atom %)	Semseyite (atom %)
Cu	0	0.02	0	0.03
Pb	85.80	51.98	49.68	23.69
Sb	0.05	27.53	0.05	21.36
Bi	0.51	0.81	0.29	0.36
S	13.35	18.52	49.96	54.56
Total	99.71	98.86	99.98	100.00

TABLE 5b. Quantitative data for the reaction galena + fluid → semseyite + fluid

Element	Galena	Factor	Initial	Semseyite	Factor	Final	Difference
Cu	0	21.00	0	0.01	0.98	0.01	0.01
Pb	0.99		20.79	9.12		8.94	-11.85
Sb	0		0	8.22		8.06	8.06
Bi	0.01		0.21	0.14		0.14	-0.07
S	1.00		21.00	21.00		20.58	-0.42

TABLE 6a. Average electron-microprobe analyses for the reaction pair semseyite, bournonite

	Semseyite (wt.%), n = 10	Bournonite (wt.%), n = 6	Semseyite (atom %)	Bournonite (atom %)
Cu	0.04	12.68	0.05	16.60
Pb	50.28	41.50	23.28	16.67
Sb	23.16	23.59	18.26	16.12
Bi	6.85	2.48	3.16	0.99
S	18.46	19.14	55.25	49.65
Total	98.79	99.39	100.00	100.03

TABLE 6b. Quantitative data for the reaction semseyite + fluid → bournonite + fluid

Element	Semseyite	Factor	Initial	Bournonite	Factor	Final	Difference
Cu	0.02	1.00	0.02	1.00	7.00	7.00	6.98
Pb	8.85		8.85	1.01		7.07	-1.48
Sb	6.94		6.94	0.97		6.79	-0.15
Bi	1.20		1.20	0.06		0.42	-0.78
S	21.00		21.00	3.00		21.00	0.00

behaviour of both elements during the formation of bournonite from semseyite. In addition, minor amounts of Pb are assumed to have been supplied during the reaction. Microprobe analyses (Table 7a) of both initial and final compositions were recalculated to 231 S

atoms (Table 7b). The reaction can thus be written as:

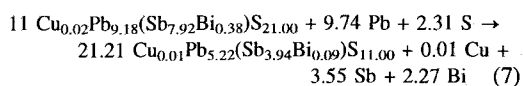


TABLE 7a. Average electron-microprobe analyses for the reaction pair semseyite, boulangerite

	Semseyite (wt.%), n = 9	Boulangerite (wt.%), n = 5	Semseyite (atom %)	Boulangerite (atom %)
Cu	0.04	0.03	0.06	0.05
Pb	52.07	55.31	23.83	25.79
Sb	26.42	24.52	20.58	19.45
Bi	2.15	0.92	0.98	0.43
S	18.44	18.02	54.55	54.29
Total	99.12	98.80	100.00	100.01

TABLE 7b. Quantitative data for the reaction semseyite + fluid → boulangerite + fluid

Element	Semseyite	Factor	Initial	Boulangerite	Factor	Final	Difference
Cu	0.02	11.00	0.22	0.01	21.21	0.21	-0.01
Pb	9.18		100.98	5.22		110.72	9.74
Sb	7.92		87.12	3.94		83.57	-3.55
Bi	0.38		4.18	0.09		1.91	-2.27
S	21.00		231.00	11.00		233.31	2.31

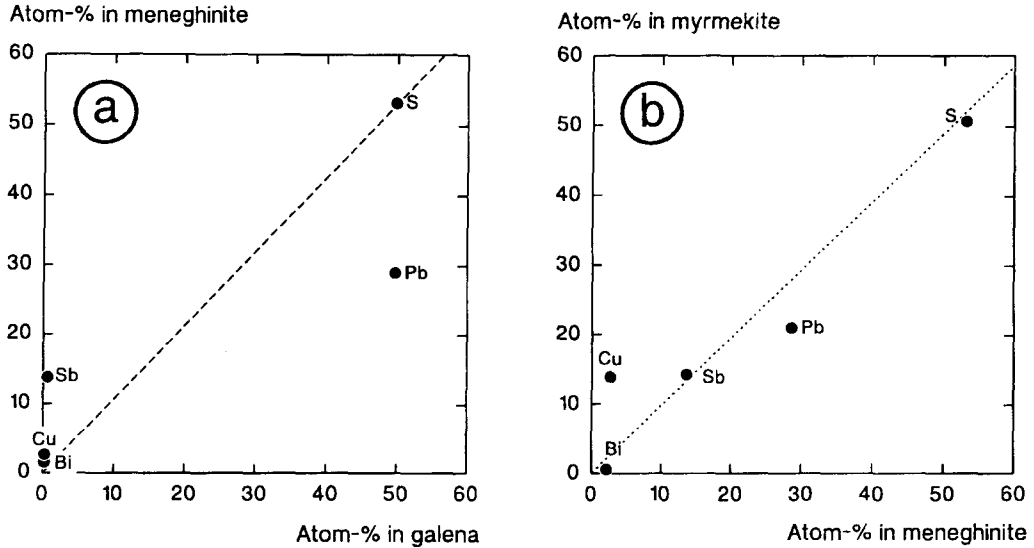
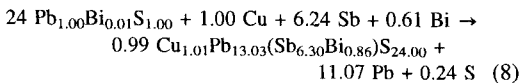


FIG. 7. Series of isocron diagrams for zoned reaction rims around galena. (a) Formation of meneghinite; reaction (8). (b) Subsequent formation of myrmekite bournonite-galena from meneghinite; reaction (9).

Another type of complex reaction rim surrounding galena, the reaction sequence *galena* → *meneghinite* → *myrmekite* (*bournonite-galena*), is very frequently texturally documented in the siderite vein and is observed in various intermediate stages. The formation of meneghinite by the reaction *galena* + *fluid* → *meneghinite* + *fluid* is the first stage of this replacement process. The isocron diagram (Fig. 7a) gives indication of an influx of Cu, Sb and Bi and a corresponding removal of Pb, assuming the relatively immobile behaviour of S. Both initial and final compositions (Table 8a) were recalculated to 24 S atoms (Table 8b). The reaction for the formation of meneghinite can be written as:



The supply of Cu and Sb is ascribed to the overprinting hydrothermal fluid of the stibnite-stage mineralization. In contrast, the source of Bi is unresolved up to now. All sulphosalts of the siderite vein, particularly meneghinite and semseyite, show major variations in their Bi-contents, ranging from values lower than 0.5 wt.% Bi up to several wt.% (Wagner and Cook, 1996). The Bi-rich varieties are restricted to particular minor areas of the vein but no relationship between such concentrations of Bi inside the vein and tectonic features has been detected. No relics of any primary Bi-rich minerals, e.g.

bismuthinite or wittichenite, have been found, and all microprobe analyses of primary (sulphide stage) galena yield Bi-concentrations which are generally lower than 1 wt.%, with a maximum frequency distribution at about 0.5–0.6 wt.%. This makes a mobilization of Bi from any primary source improbable.

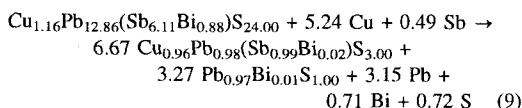
Most meneghinite has decomposed in a second replacement process to a myrmekitic assemblage of bournonite and galena. The resulting mineral reaction *meneghinite* + *fluid* → *bournonite* + *galena* + *fluid* has been previously described by Ni Wen *et al.* (1991) from a siderite-hosted vein mineralization from Dhurode, Co. Cork, Ireland. In contrast to the results of these authors, in which a relatively immobile behaviour of Pb and Sb was identified, the isocron diagram (Fig. 7b) for the same reaction in the Apollo mine indicates relative immobility of Sb and S. This is, however, in excellent agreement with the behaviour of both elements in all other second step replacement processes at Apollo as discussed above. A significant supply of Cu and loss of Pb and minor amounts of Bi can also be deduced from this isocron diagram. Microprobe data for the reaction pair, other quantitative data for the reaction and volume data for the myrmekitic intergrowth are given in Tables 9a,b and c respectively. Both initial and final (product) compositions were recalculated to 24 S-atoms. The resulting overall reaction can be written as:

TABLE 8a. Average electron-microprobe analyses for the reaction pair galena, meneghinite

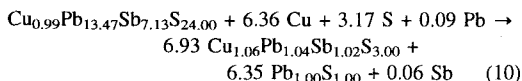
	Galena (wt.%), n = 5	Meneghinite (wt.%), n = 6	Galena (atom %)	Meneghinite (atom %)
Cu	0.05	1.43	0.10	2.24
Pb	86.06	60.16	49.78	28.83
Sb	0.01	17.09	0	13.94
Bi	0.44	4.00	0.25	1.90
S	13.34	17.15	49.87	53.11
Total	99.90	99.83	100.00	100.02

TABLE 8b. Quantitative data for the reaction galena + fluid → meneghinite + fluid

Element	Galena	Factor	Initial	Meneghinite	Factor	Final	Difference
Cu	0	24.00	0	1.01	0.99	1.00	1.00
Pb	1.00		24.00	13.03		12.93	-11.07
Sb	0		0	6.30		6.24	6.24
Bi	0.01		0.24	0.86		0.85	0.61
S	1.00		24.00	24.00		23.76	-0.24



For the purposes of comparison the reaction of Ni Wen *et al.* (1991) has been rearranged to give:



Our data are not in full agreement with those of Ni Wen *et al.* (1991) concerning the mobility and immobility of specific elements involved into the breakdown of meneghinite. This discrepancy and also the results of Moëlo *et al.* (1988) suggests that general trends cannot be readily established; the factors governing element behaviour during complex replacement reactions varying significantly from case to case. We would endorse the comments of Ni Wen *et al.* (1991) that future observations of this type may yet lead to the establishment of underlying patterns, given the relatively limited state of knowledge, at present, concerning such reaction mechanisms.

### Discussion

*Fluid evolution.* Comparison of the mobile and immobile behaviour of certain elements during the various replacement reactions discussed above leads

to the recognition of distinct patterns. The first stage of each replacement sequence of the siderite vein is characterized by a supply of major amounts of Sb and minor Cu, which is ascribed to the introduction of new (stibnite stage) hydrothermal fluids into the pre-existing vein system. At the same time, the quartz-stibnite vein system shows simple precipitation of stibnite, presumably because the activity of Pb in the hydrothermal fluid at the beginning of the mineralization was low. A strong disequilibrium between the primary sulphides and the mineralizing hydrothermal fluid is considered as the driving force for the formation of the first generation of sulphosalts; tetrahedrite, semseyite and meneghinite.

The second stage of the replacement processes of the siderite vein displays a contrasting pattern, and the isocon diagrams of all mineral reactions of this stage indicate the relatively immobile behaviour of Sb and S. A directly comparable immobile behaviour of both elements has been reported by Moëlo *et al.* (1988) for the reaction *berthierite + fluid* → *jamesonite + stibnite + fluid*. The same reaction has been treated by Ni Wen *et al.* (1991) in a quantitative manner and plotted on an isocon diagram, with the result of a near-ideal two-element isocon of Sb and S and the assumption of an influx of Pb and a loss of Fe during the reaction process.

During this second stage of the replacement process in the Apollo vein systems, reactions affecting Pb-rich sulphosalt minerals are character-

TABLE 9a. Average electron-microprobe analyses for the reaction pair meneghinite, bournonite + galena

	Meneghinite (wt.%), n = 5	Bournonite (wt.%), n = 2	Galena (wt.%), n = 1	Meneghinite (atom %)	Bournonite (atom %)	Galena (atom %)
Cu	1.67	12.55	0.10	2.58	16.18	0.19
Pb	60.21	41.54	84.87	28.57	16.41	49.02
Sb	16.81	24.67	0.03	13.58	16.60	0.02
Bi	4.16	0.82	0.65	1.96	0.32	0.38
S	17.38	19.77	13.50	53.32	50.49	50.39
Total	100.23	99.35	99.15	100.01	100.00	100.00

TABLE 9b. Quantitative data for the reaction meneghinite + fluid → bournonite + galena + fluid

Element	Meneghinite	Factor	Initial	Bournonite	Factor	Galena	Factor	Final	Difference
Cu	1.16	1.00	1.16	0.96	6.67	0	3.27	6.40	5.24
Pb	12.86		12.86	0.98		0.97		9.71	-3.15
Sb	6.11		6.11	0.99		0		6.60	0.49
Bi	0.88		0.88	0.02		0.01		0.17	-0.71
S	24.00		24.00	3.00		1.00		23.28	-0.72

TABLE 9c. Volume data for the reaction meneghinite + fluid → bournonite + galena + fluid

	Meneghinite	Bournonite	Galena
Volume % in myrmekite		84.43	15.57
Volume per 24 S Atoms (Å <sup>3</sup> )	1128.4	1111.6	1255.2
% in myrmekite on 24-S basis		85.96	14.04

ized by a loss of Pb and supply of Cu, whereas Cu-rich minerals, especially tetrahedrite, display the opposite behaviour with a loss of Cu and supply of Pb. This contrasting behaviour between the two geochemically distinct local subsystems, both of which are in contact with the mineralizing fluid, can be interpreted as the first step towards equilibration of geochemical differences within the whole system. After the system had adjusted and reacted to the introduction of Sb and Cu by the overprinting hydrothermal fluid, and the disequilibrium between fluid and solid compositions was, at least partly, diminished, the geochemical contrasts between different segments of the vein took on a dominant role. Additionally, a second contrast in geochemistry existed between the Pb-rich sulphosalt phases of the siderite vein and the Pb-free stibnite-dominated assemblage of the quartz-stibnite vein system.

Although a major part of the Pb released during replacement of the Pb-rich sulphosalts of the siderite vein was probably consumed during the formation of bournonite from tetrahedrite, a general enrichment of Pb in the mineralizing fluid can be assumed, based on the proportions of mineral phases quantitatively observed in polished section. The formation of increasingly Pb-rich sulphosalts in the quartz-stibnite vein system can, therefore, be ascribed to an increasing disequilibrium between stibnite and the by now Pb-rich hydrothermal fluid phase. A contemporaneous slight increase in the activity of Sb in the hydrothermal fluid during the decomposition of stibnite can be deduced from the isocon diagrams constructed for both reactions of the quartz-stibnite vein system. The ultimate destination of this Sb is still unresolved, although a weak dispersion halo with mean concentrations of  $21 \pm 1$

ppm Sb in the footwall and  $36 \pm 1$  ppm in the hanging wall rock may indicate a final loss of Sb from the vein into the host rocks.

The mineral reactions discussed above and the mineral chemistries of the sulphosalt phases of the stibnite-stage mineralization indicate that the primary composition of the mineralizing hydrothermal fluid at the time of its introduction into the system was Sb-, (Bi-) and Cu-rich and Pb-, As- and Ag-poor. Minerals which commonly show an As-substitution in their structures, such as tetrahedrite, bournonite and pyrite are almost free of As. The Ag-poor character of the hydrothermal fluid is concluded from the compositions of tetrahedrite and other Cu-bearing Pb-Sb-(Bi)-sulphosalts, which show very low Ag-contents, generally below 0.5 wt.%, and the absence of any Ag-Sb or Ag-Pb-Sb sulphosalts. The activity of Sb in the hydrothermal fluid at the beginning of the mineralizing event must have been relatively high, and the formation of meneghinite and tetrahedrite shows that minor amounts of Cu must have been present in the fluid at that time. The incomplete character of all mineral reactions in the first stage of the replacement sequence indicates a relatively rapid decrease in the activity of Sb in the fluid. Furthermore, a stagnation of the fluid inside the vein system must be assumed to have taken place in order to explain the observed evolution of fluid composition. A constant supply of Sb-rich fluids would most likely have resulted in more complete reactions, a consumption of all Pb and Cu of the primary sulphides, and afterwards, in a precipitation of stibnite in the siderite vein. The slight increase of the activity of Sb during the later replacement of stibnite in the quartz-stibnite vein system is, however, considered as being too low to have made a significant influence upon the overall fluid composition.

Intensive pyritization of the host rocks of both the siderite vein and the quartz-stibnite vein system can be explained either by their interaction with an initially Fe-rich hydrothermal fluid or by the mobilization of Fe during the decomposition reaction chalcopyrite  $\rightarrow$  tetrahedrite. The second alternative is strongly supported by the precipitation of second generation pyrite after the formation of tetrahedrite and the mobilization of primary sphalerite. Assuming this to be a realistic interpretation, the resulting fluid evolution is characterized by a significant increase of the activity of Fe in the fluid after the introduction into the vein system, and a rapid decrease after the precipitation of the pyrite. This is concordant with the absence of both gudmundite, FeSbS, and berthierite, FeSb<sub>2</sub>S<sub>4</sub>.

Significant amounts of Bi must have been present within the hydrothermal fluid at the initiation of the mineralizing event, because the first generation of

sulphosalts in the siderite vein, especially meneghinite, jaskolskiite and semseyite, displays high concentrations of Bi. In contrast, the Pb-Sb-sulphosalts of the quartz-stibnite vein system are extremely poor in Bi with concentrations lower than 0.5 wt.% (Wagner and Cook, 1996). This contrasting behaviour can be explained by a rapid decrease in the activity of Bi in the fluid after the formation of the Bi-rich sulphosalts in the siderite vein. Formation of sulphosalts inside the quartz-stibnite vein system was not possible at the beginning of the sulphidic mineralization episode, because the activity of Pb in the hydrothermal fluid was generally too low. Primary galena supplied the Pb necessary for the formation of Bi-rich (Cu)-Pb-Sb-sulphosalts in the siderite vein and the replacement reactions also resulted in a continuing increase of the activity of Pb in the fluid. The mobilization of primary sphalerite and the reprecipitation as Fe-poor second generation sphalerite resulted in an initial increase, followed by a later rapid decrease, of the overall activity of Zn in the hydrothermal fluid.

In contrast to the oscillatory behaviour of the activities of metals in the fluid, a nearly constant high sulphur activity during the entire hydrothermal overprinting event can be assumed. This is because sulphides have continuously formed until the termination of mineralization and neither native antimony nor antimonides have been observed. The initial formation of chlorite and quartz without sulphides can most easily be explained by the relatively high formation temperatures of these minerals, thus avoiding the more complicated assumption of an initial S-poor fluid composition and a later supply of sulphidic fluids. Both fluid inclusion data on quartz and geothermometric calculations based on the composition of vein chlorite indicate 390–410°C as starting temperatures for the precipitation of quartz and chlorite, and 240–260°C at the end of quartz growth (Wagner, 1996). Formation of stibnite and sulphosalts should not have occurred at these higher temperatures; experimental determinations of solubility products of antimony (Krupp, 1988; Spycher and Reed, 1989) and theoretical calculations (Munoz *et al.*, 1992) indicate that stibnite precipitation is possible only at temperatures below about 250°C. These calculations are based on initial Sb concentrations in the hydrothermal fluid comparable to those typically found in recent geothermal waters (Munoz *et al.*, 1992), with no need for a pre-concentrated source of Sb in certain sediments (e.g. graphitic black shales).

To summarize the above discussion, two principal factors are considered to control the evolution of fluid composition. The first one is, of course, the primary composition of the hydrothermal fluid at the time of its introduction into the vein system. This initial

composition defines the extent (degree) of disequilibrium between the fluid composition and the composition of the pre-existing vein mineral assemblages and, therefore, the possibility for mineral reactions and diffusion processes to take place. After the fluid has reached the vein system, however, the second controlling factor becomes important. The primary fluid composition is modified by interactions with the minerals of the vein. In addition, geochemical contrasts between various spatially distinct localities inside the vein, which can be regarded as local subsystems within a larger system, lead to chemical gradients for certain elements in the hydrothermal fluid. This results in mass transfer between the geochemically contrasting areas and a continuing equilibration process throughout the whole system. The interdependence of fluid and solid composition results in oscillatory behaviour of the activities of certain elements in the hydrothermal fluid.

**Reaction mechanisms.** Textural relationships displayed by the minerals involved in the various replacement processes at Apollo mine reveal that grain boundaries have acted as fluid channels and as first order reaction interfaces. This is especially valid for grain boundaries between a mineral phase involved in a certain reaction and another phase which is not involved, e.g. the boundary galena-pyrite during the formation of semseyite from galena. Grain-boundary diffusion must, therefore, be considered to be a reaction mechanism of major importance which could have enabled a relatively fast transport of mobile components to take place.

The reactive replacement processes of the solid phases themselves are considered to have been controlled by solid-state diffusion, which has been shown to be of major importance in the development of chalcopyrite disease in sphalerite (Bente and Doering, 1993; 1995). Further examples of solid state diffusion between ore minerals include interdiffusion of S and Se between tiemannite, HgSe and cinnebar, HgS (Boctor and Brady, 1980). Because the behaviour of certain elements in mineral reactions (1) to (10) in this paper is in good agreement with the assumption of a relative immobility of S, the classical model of diffusion in sulphides (Birchenall, 1974), in which mobile cations move through a rigid sulphur lattice, is applicable. Some minor modifications have, however, to be considered with respect to the complexity of the crystal structures of the sulphosalt minerals involved in these reactions. The principles underlying the crystal structures of sulphosalt minerals (Makovicky, 1985; 1989) possess some general features which should favour solid-state diffusion processes. The more complicated structures, in particular, possess certain interfaces between rods or layers of simpler structure types, which can be derived from the PbS and the SnS structures.

These structural interfaces represent discontinuities inside the lattice and should, therefore, be able to act as diffusion interfaces during the replacement processes. The cations in the direct environment of these interfaces are especially energetically favoured to leave the lattice by diffusion. Moreover, some sulphosalt structures like zinkenite and its derivatives, possess channels in their structures which can be filled with non-stoichiometric quantities of cations (Lebas and Le Bihan, 1976; Smith, 1986). These must be considered to play a dominant role in the replacement of these minerals.

Finally, and probably most importantly, a simple diffusion of ionic or complex species driven by concentration gradients in the hydrothermal solution, can be assumed to have been the fundamental mechanism enabling mass transport over wider distances, especially between the siderite vein and the quartz-stibnite vein system.

## Conclusions

1. Reactive replacement of sulphide and sulphosalt minerals in the siderite vein has proceeded in two reaction steps. Isocon diagrams for all individual reactions indicate the relative immobility of S during the first stage of the replacement process, and relative immobility of both S and Sb during the subsequent second stage. Mineral reactions of the quartz-stibnite vein system are characterized by the immobile behaviour of S.

2. The first stage of reaction is dominated by the formation of sulphosalts from primary sulphides, and diminution of the disequilibrium between the pre-existing mineral phases and the Sb-, Bi- and Cu-rich, and As-, Ag- and Pb-poor hydrothermal fluids introduced into the siderite vein.

3. The second stage is controlled by equilibration processes between geochemically contrasting areas of the vein systems, which are considered as local subsystems of the overall system.

4. Hydrothermal fluid evolution is controlled by the primary composition of the fluid at its time of introduction into the vein system, and by interactions with the pre-existing solid mineral phases of the veins.

5. Solid-state diffusion and grain-boundary diffusion are considered to be the reaction mechanisms controlling the short-range transport of mass in the replacement processes, whereas diffusion of ionic or complex species through the solution is probably the dominant process for long-range transport.

## Acknowledgements

The assistance of Herr P. Spaethe with preparation of polished sections is gratefully appreciated. Herr K.-P.

Kelber is thanked for the black-and-white photographs.

### References

- Behr, H.J., Horn, E.E., Frentzel-Beyme, K. and Reutel, C. (1987) Fluid inclusion characteristics of the Variscan and post-Variscan mineralizing fluids in the Federal Republic of Germany. *Chem. Geol.*, **61**, 273–85.
- Bente, K. and Doering, T. (1993) Solid-state diffusion in sphalerites: an experimental verification of the chalcopyrite disease. *Eur. J. Mineral.*, **5**, 465–78.
- Bente, K. and Doering, T. (1995) Experimental studies on the solid state diffusion of Cu and In in ZnS and on 'disease', DIS (Diffusion Induced Segregations), in sphalerite and their geological applications. *Mineral. Petrol.*, **53**, 285–305.
- Birchennall, C.E. (1974) Diffusion in sulfides. In *Geochemical Transport and Kinetics* (A.W. Hofmann, B.J. Giletti, H.S. Yoder, Jr. and R.A. Yund, eds.), Carnegie Institution of Washington, Publication 634, 53–9.
- Boctor, N.Z. and Brady, I.M. (1980) Interdiffusion of S and Se in tiemannite. *Carnegie Inst. Washington Year Book*, **78**, 580–2.
- Boiron, M.C., Cathelineau, M., Dubessy, J. and Bastoul, A.M. (1990) Fluids in Hercynian Au veins from the French Variscan belt. *Mineral. Mag.*, **54**, 231–43.
- Couto, H., Roger, G., Moëlo, Y. and Bril, H. (1990) Le district à antimoine-or Durico-Beirao (Portugal): évolution paragénetique et géochimique; implications métallogéniques. *Mineral. Dep.*, **25**, 69–81.
- Fenichel, W., Gies, H., Gleichmann, H.D., Helmind, W., Hentschel, H., Heyl, K.E., Hüttenhain, H., Langenbach, U., Lippert, H.J., Luznat, M., Meyer, W., Pahl, A., Rao, M.S., Reichenbach, R., Stadler, G., Vogler, H. and Walther, H.J. (1985) Die Sideritergänge im Siegerland-Wied-Distrikt. *Geolog. Jahrb. Reihe D*, **77**, 1–517.
- Franke, W. and Oncken, O. (1990) Geodynamic evolution of the North-Central Variscides - a comic strip. In *The European Geotraverse: Integrative Studies*, European Science Foundation, Strasbourg, 187–94.
- Grant, J.A. (1986) The isocon diagram - a simple solution to Gresens's equation for metasomatic alteration. *Econ. Geol.*, **81**, 1976–82.
- Gresens, R.L. (1967) Composition-volume relationships of metasomatism. *Chem. Geol.*, **2**, 954–71.
- Hein, U.F. (1993) Synmetamorphic Variscan siderite mineralization of the Rhenish Massif, Central Europe. *Mineral. Mag.*, **57**, 451–67.
- Koenigswald, W. von and Meyer, W. (1994) *Erdgeschichte im Rheinland*. Fossilien und Gesteine aus 400 Millionen Jahren. Pfeil-Verlag, München, 240 pp.
- Krupp, R.E. (1988) Solubility of stibnite in hydrogen sulfide solutions, speciation, and equilibrium constants, from 25 to 350°C. *Geochim. Cosmochim. Acta*, **52**, 3005–3015.
- Lebas, G. and Le Bihan, M.T. (1976) Etude chimique et structurale d'un sulfure naturel: la zinckénite. *Bull. Soc. Fr. Mineral. Cristallogr.*, **99**, 351–60.
- Makovicky, E. (1985) The building principles and classification of sulphosalts based on the SnS archetype. *Fortschr. Mineral.*, **63**, 45–89.
- Makovicky, E. (1989) Modular classification of sulphosalts - current status. Definition and application of homologous series. *Neues Jahrb. Mineral. Abh.*, **160**, 269–97.
- Meyer, W. (1965) Gliederung und Altersstellung des Unterdevons südlich der Siegener Hauptüberschiebung in der Südost-Eifel und im Westerwald (Rheinisches Schiefergebirge). *Max-Richter-Festschrift*, Clausthal-Zellerfeld, 35–47.
- Moëlo, Y., Robert, J.F. and Picot, P. (1988) Symplectite jamesonite-stibine de la mine d'antimoine de Fecunda (district du Val de Ribes, Pyrénées catalanes). *Bull. Mineral.*, **111**, 451–5.
- Munoz, M., Courjault-Rade, P. and Tollon, F. (1992) The massive stibnite veins of the French Paleozoic basement: a metallogenic marker of Late Variscan brittle extension. *Terra Nova*, **4**, 171–7.
- Ni Wen, N., Ashworth, J.R. and Ixer, R.A. (1991) Evidence for the mechanism of the reaction producing a bournonite-galena symplectite from meneghinite. *Mineral. Mag.*, **55**, 153–8.
- Oncken, O. (1984) Zusammenhänge in der Strukturgenese des Rheinischen Schiefergebirges. *Geol. Rdsch.*, **73**, 619–49.
- Ortega, L. and Vindel, E. (1995) Evolution of ore-forming fluids associated with late Hercynian antimony deposits in Central/Western Spain: case study of Mari Rosa and El Juncalón. *Eur. J. Mineral.*, **7**, 655–73.
- Perichaud, J.J. (1980) L'antimoine, ses minerais et ses gisements. Synthèse géologique sur les gisements du Massif Central français. *Chron. Rech. Min.*, **456**, 1–64.
- Smith, P.P.K. (1986) Direct imaging of tunnel cations in zinkenite by high-resolution electron microscopy. *Amer. Mineral.*, **71**, 194–201.
- Spycher, N.F. and Reed, M.H. (1989) As(III) and Sb(III) sulfide complexes: An evaluation of stoichiometry and stability from existing experimental data. *Geochim. Cosmochim. Acta*, **53**, 2185–94.
- Wagner, T. (1996) *Die Antimon-Mineralisation der Grube Apollo im Siegerland-Wieder Spateisenbezirk*. Unpublished Diploma Thesis, Univ. Würzburg, 176 pp.
- Wagner, T. and Cook, N.J. (1996) Bismuth-antimony sulfosalts from siderite-hosted vein mineralization, Apollo mine, Siegerland, FRG. *Neues Jahrb.*

*Mineral. Abh.*, **171**, 135–53.

Walther, H.W. (1982) Die varistische Lagerstättenbildung im westlichen Mitteleuropa. *Z. dt. geol. Ges.*, **133**, 667–98.

Weber, K. and Behr, H.J.: (1983) Geodynamic interpretation of the Mid-European Variscides. In

*Intracontinental Fold Belts* (H. Martin and F.W. Eder, eds). Springer Verlag, Berlin-Heidelberg, 427–59.

[*Manuscript received 10 September 1996; revised 15 January 1997*]